Enhancement of spin-to-charge conversion of diamond NV centers at ambient conditions using surface electrodes

Liam Hanlon ⓘ, Michael Olney-Fraser ⓘ, and Marcus W. Doherty[*]

Department of Quantum Science and Technology, Research School of Physics, Australian National University, Canberra ACT 2601, Australia

Lukas Razinkovas ⓘ

Department of Fundamental Research, Center for Physical Sciences and Technology (FTMC), Vilnius LT-10257, Lithuania

The nitrogen-vacancy (NV) center in diamond is a heavily studied defect due to its potential applications to quantum metrology and computation, particularly in ambient conditions. The key mechanism to using the NV in any application lies in the ability to read out the spin state of the defect which is typically done optically. The optical contrast is then the key metric for electron spin readout fidelity and one of the key limiting factors in the NV's overall performance. We present a mechanism for high contrast readout using the spin-to-charge conversion mechanism in conjunction with an electrode to improve the spin contrast by altering the NV energy levels relative to the diamond conduction band. Theoretical modeling predicts an optical spin contrast at 42% which would be the highest optical contrast for the NV at room temperature and the technique opens up a range of alternative research pathways for the NV which are discussed.

I. INTRODUCTION

The nitrogen-vacancy (NV) center defect in diamond shows great promise as a tool for a variety of quantum applications including metrology and imaging [1–5] as well as computing and networking [6–10]. The defect is easy to engineer, can be manipulated with simple laser and microwave pulse sequences, and can be designed in a variety of forms by shaping the diamond structure that houses the defect [11–15]. Arguably the most impressive quality of the NV center is its ability to initialize, manipulate, and read out quantum states in ambient conditions [11]. This capability vastly increases the NV's applicability compared to other technologies, allowing for (among many other applications) powerful sensors of biological samples and room temperature quantum computers.

One of the major drawbacks of the NV center is its low electron spin optical contrast and associated readout fidelity. The low contrast limits the sensitivity of an NV sensor and the overall computational fidelity of an NV quantum computer. In addition to this, under optical illumination, the NV can photoionize, changing its charge state from NV^- to NV^0, a state that does not have the same optical spin initialization and readout mechanisms. In this case, the NV needs to be converted back into the NV^- state via optical recombination from the diamond valence band [16]. However, this ability to alter the NV charge state allows for the development of the spin-to-charge conversion (SCC) protocol, where the NV spin state is mapped to the NV charge state and the spin state is read out via a much higher fidelity charge state readout protocol. There have been many SCC protocols developed at cryogenic temperatures [17–19] and in ambient conditions [20,21]. Cryogenic SCC protocols perform better, but cannot work in ambient conditions, removing one of the NV's most useful advantages. While the ambient SCC protocols are more applicable, their improvement is modest and does not address the issue of unintended ionization for true charge state control in the NV.

We introduce a SCC protocol at ambient conditions with the application of an electrode over a near-surface NV to facilitate efficient photoionization from the lower singlet state of the NV^- (Fig. 1). The SCC protocol presented in this work is largely inspired by Hopper *et al.* [21]; in their work, near-infrared (1064 nm) lasers were used with conventional optics to pump electron population in the NV into the singlet state and ionize the defect using the near-infrared laser. The main difficulty ionizing from the NV lower singlet is cross-talk in the NV. The predicted energy gap from the lower singlet state to the diamond conduction band is about 570 nm (2.1 eV) [16]. In ambient conditions, a 570 nm laser has a high chance of exciting the NV triplet transition as well as the ionization transition due to its broad absorption sideband [22]. This cross-talk will create noise in the spin initialization as well as the charge state readout. To avoid cross-talk, Hopper *et al.* used the 1064 nm laser to perform quadratic ionization. While the rate of triplet excitation is very low at this energy, the rate of ionization is also low, reducing the chances of a successful spin-to-charge conversion. The optical spin contrast achieved was about 25%, equivalent to that of conventional optical spin cycling techniques [20,23].

The purpose of the electrode in our work is to apply an electric potential that shifts the NV energy levels relative to the diamond conduction band [Fig. 1(b)]. Positive potentials will shift the energy levels closer to the conduction
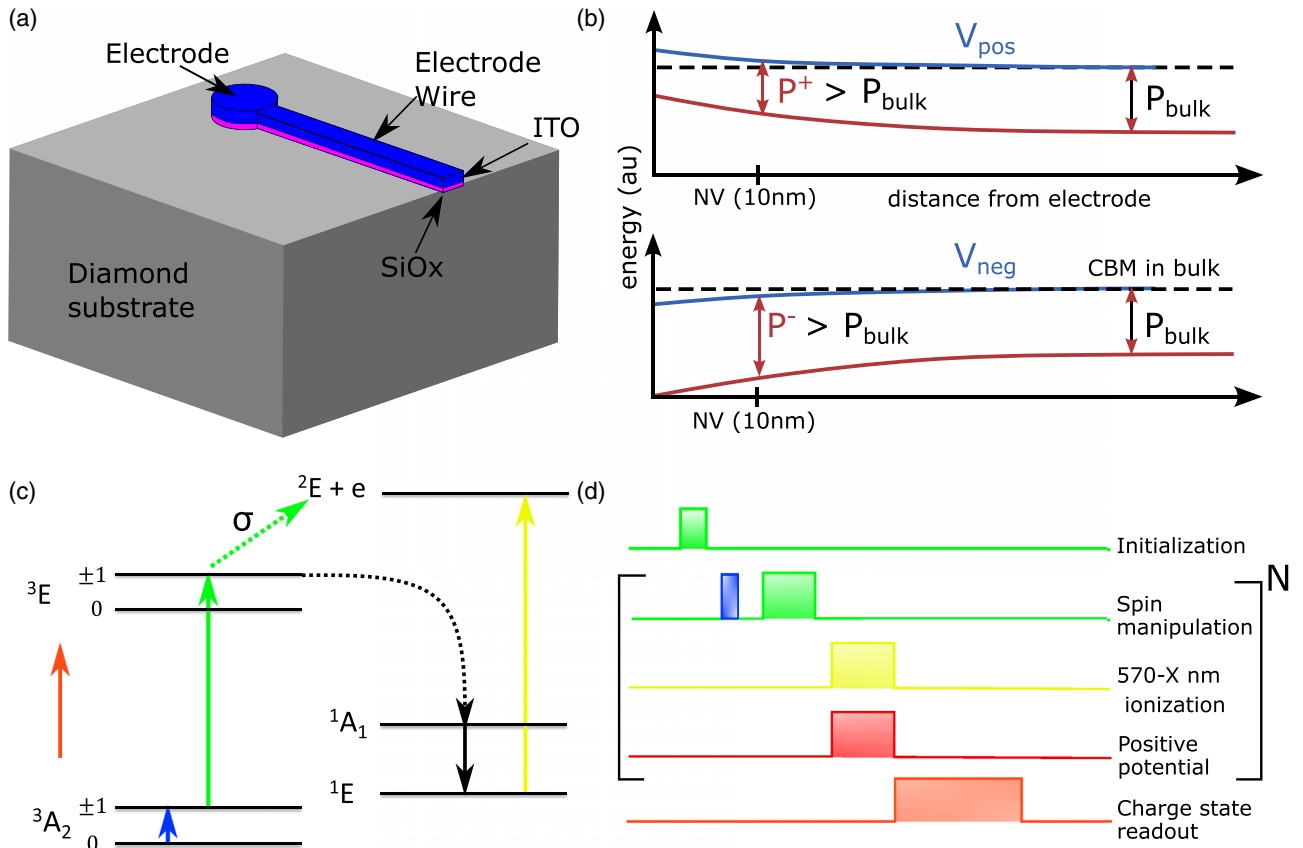
*mwdoherty@anu.edu.au

134111-1

FIG. 1. (a) Image of the cylindrical electrode over a near-surface NV (10 nm deep) and the electrode wire that connects to a power supply, providing the electrode potential. (b) Diagram of the electrode effect on the energy structure. The first image is with a positive electrode potential (V_{pos}) which shifts the conduction band and NV energy levels upwards compared to the CBM in bulk diamond with no potential. This reduces the photoionization energy gap P^+ compared to the bulk case with no potential (P_{bulk}). In the second image, a negative potential shifts the energy levels downwards compared to the bulk CBM, widening the energy gap P^-. (c) Energy diagram depicting the SCC protocol. The NV is initialized into the ^1E singlet state with a green pump laser and a microwave π pulse (blue) for spin manipulation. It is then ionized with a high power yellow laser into the NV^0 ^2E state with an electron in the diamond conduction band. The charge state of the NV is then read out with a 595 nm orange laser pulse. This sequence also features the quadratic ionization from the ^3E state to the conduction band which has a cross-section ratio of σ. The pulse sequence for the same SCC protocol in (c) is shown in (d) and includes the pulsing for the electrode itself, where the positive potential is turned on during the ionization phase. The brackets with the value N indicate a section that can be repeated for better contrast considered in Sec. III.

band, increasing photoionization probability, whereas negative potentials will have the opposite effect. The change in the energy gap from the NV energy levels to the diamond conduction band is due to the different ways that the two structures are affected by the electrode potential. The diamond conduction band will feel an averaged effect of the potential which can be modeled using effective mass theory and the NV can feel a much larger potential at a point in space as it is an atomic defect. This allows us to selectively change the ratio of photoionization to initialization cross section in order to maximize or minimize ionization from any energy level in the NV. By adding a potential that ionizes the NV energies towards the diamond conduction band, the singlet ionization energy gap can go below 2.0 eV. If the ionization energy gap is small enough, then the triplet absorption cross section will be effectively zero at the same energy, allowing for a higher probability ionization with low levels of cross-talk and a high optical spin contrast which we can calculate.

In this paper, the experimental design is outlined and the SCC contrast is calculated using rate equation modeling [24], the results of which are compared to another established ambient SCC protocol [20]. These results are critically analyzed and some alternate applications of the electrode are considered.

II. EXPERIMENTAL DESIGN AND CONTRAST

We design our experimental setup with a cylindrical electrode fabricated over an NV and a thin wire connecting to a voltage source [Fig. 1(a)]. The electrode and wire have a thin, insulating silicon oxide (SiOx) layer to prevent charges from moving from the diamond into the electrode. The electrode itself is a transparent indium-tin oxide (ITO) conductive layer that carries the electric potential and allows for optical illumination through the electrode. The electrode changes the energy levels in the diamond band structure which can be

calculated using effective mass theory. The electrode will also alter the NV energy levels, but to a greater effect than the conduction band energy levels [Fig. 1(b)]. See Supplemental Material A1 [25] for more details of the electrode effects on the energy levels [17,26–32].

The SCC protocol is shown in Figs. 1(c) and 1(d), which are very similar to the protocol from Hopper *et al.* [21]. A green laser pulse initializes the NV into the $m_s = 0$ spin state and a combination of green laser and microwave excitation pumps the defect in the desired excited state spin level. Population in the $m_s = \pm 1$ state preferentially decays via the intersystem crossing (ISC) into the NV singlet states, while $m_s = 0$ states preferentially decay to the ground state. When the electron population is in the relatively long lifetime lower singlet state (≈ 200 ns [32]), a powerful, nonresonant ionization pulse is applied to ionize the defect. In this setup, the $m_s = 0$ spin state is mapped to the NV$^-$ charge state and the $m_s = \pm 1$ is mapped to the NV^0 charge state. At the end of the sequence, the charge state is read out with a 595 nm orange laser pulse. During the ionization phase, the electrode has a positive potential to shift the energy levels closer to the diamond conduction band [Fig. 1(b)] and increase the ionization rate. This short period of electrical manipulation (approximately 50 ns, the time period of the ionization) means that the spin manipulation occurs in the absence of the electrode potential. This allows for spin manipulation that is not affected by the electrode as an external potential can cause spin mixing. It also means that the NV can be further manipulated with other external fields like a bias magnetic field. Additionally, other short electrode pulses can be added to the protocol which is considered in the Discussion Sec. IV. While electrode pulses on the nanosecond scale are difficult, it is not impossible using modern electronics [33,34].

If the electrode potential shifts the NV energy levels such that there is no cross-talk available between the ionization and triplet excitation energies, then the optical contrast can be calculated using rate equation modeling. The rate model consists of five NV energy levels (where the $^1A_1$ state is removed due to its low lifetime [27]) plus a single level for the ionized state. Transition rates between the states form a 6×6 matrix used in the rate model where the excitation/ionization laser power and pulse times are free variables to optimize and the remaining constants can be found in literature [29,30]. Note that the microwave pulse that performs the spin manipulation is implicit in this model and is assumed to excite with 100% probability [26]. We also assume that the NV can be initialized into a particular spin state with 100% fidelity. While this is not precisely true, it can be achieved with near-unity fidelity with careful manipulations [28]. See Supplemental Material A2 [25] for a more detailed description of the rate equation model [11,22,35–37].

In order to solve the rate equation we need the ratio of the triplet absorption to photoionization cross section, σ [Fig. 1(c)]. This value tells us the probability of an electron being raised to the excited triplet state or ionized into the diamond conduction band during the pumping phase. Ideally, σ should be as low as possible to prevent triplet ionization of the $m_s = 0$ state, lowering spin contrast. This value is typically set by the intrinsic properties of the NV but can be theoretically altered with a two-step electrode potential, where
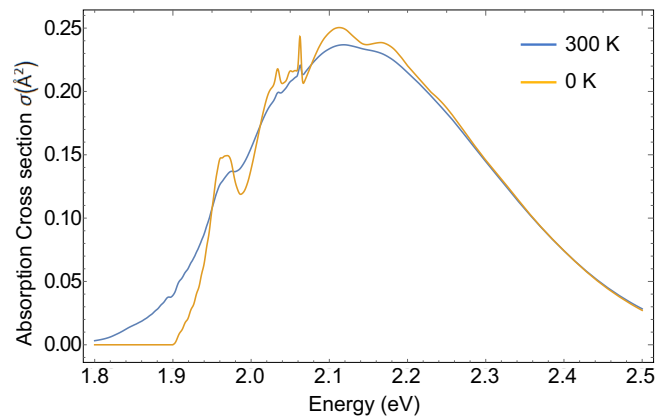

FIG. 2. Plot of the absorption cross section calculated using Huang-Rhys theory. The yellow curve is the solution at 0 K and is a match for the absorption cross-section data shown in Razinkovas *et al.* [22]. The blue curve is the same calculation performed at 300 K. At higher temperatures, the data broadens and lowers slightly in amplitude which is expected.

the electrode has a negative potential during the pumping phase but a positive potential during the ionization phase. This is discussed in more detail in Sec. IV.

To work out σ, the ratio of the absorption triplet cross section and the triplet photoionization cross section is taken for a given excitation energy. To achieve this we need to calculate the triplet absorption sideband of the NV and compare it to the photoionization cross section. Note that the ratio is the key data, not the cross section itself; this means that the units are not important as long as they are the same across the two data sets. We studied the absorption cross section at room temperature by applying a similar calculation from Davies *et al.* [11,35,38] which uses the Frank-Condon theory of electronic and vibrational interactions during an electronic transition along with the Huang-Rhys model of transitions in a defect. The theory states that with a temperature-dependent electron-phonon coupling, the function that describes the vibrational overlap is given by

$$F(\omega, T) = e^{-S} \sum_{i=1}^{\infty} \frac{S^i}{i!} F_i(\omega, T), \qquad (1)$$

where S is the average Huang-Rhys factor which is a measure of the interaction of defect electrons with phonons in a crystal lattice [36,37] and $F_i(\omega, T)$ is the temperature-dependent function describing the vibrational overlap of an electronic transition with i phonons. Equation (1) can be solved for any number of phonon interactions and different temperatures to create a phonon sideband. See Supplemental Material A3 [25] for more details on this calculation [11,22,35–37].

Figure 2 shows the absorption spectrum for the NV across a range of photon energies with the zero phonon line (ZPL) omitted. The yellow curve shows the calculated absorption spectrum at 0 K which is the same as the data reported in Razinkovas *et al.* [22]. The blue curve shows the same absorption spectrum calculated at 300 K. As expected, the data is largely the same, but the higher temperature electron-phonon interactions broaden the absorption spectrum. From this data,
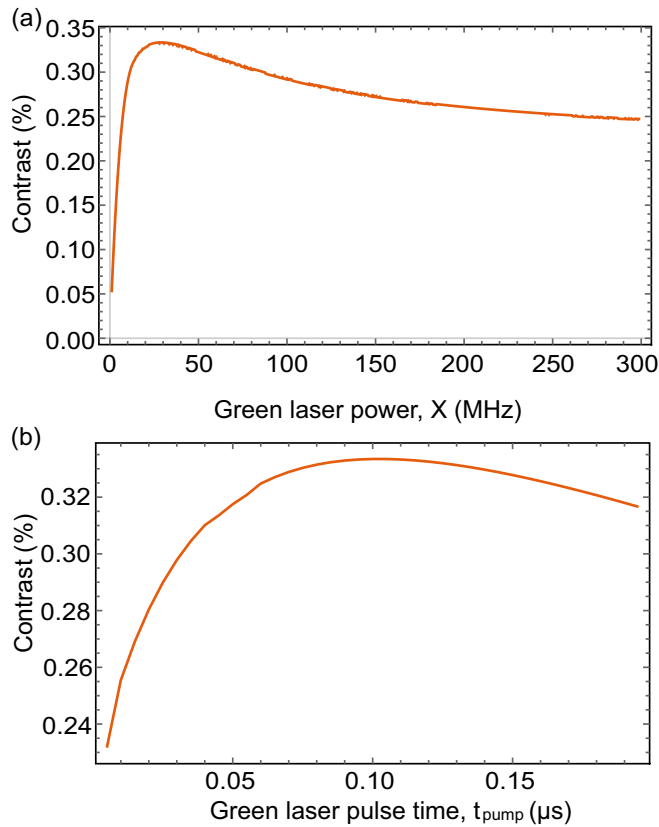
FIG. 3. Plot of the optical spin contrast optimization as a function of (a) green laser excitation and (b) green laser pulse duration for the pumping phase. All other parameters are optimized to give the largest optical contrast. In both plots, the contrast steadily increases until reaching an optimum value of 33% before decreasing.

the cross section for absorption can be compared to the cross section for photoionization from Razinkovas *et al.* [22] at 2.3 eV (532 nm) to obtain a ratio of ≈0.26. This ratio is then used as the σ value in the rate equation modeling. This plot can also be used as a rough understanding of the energy shift required to reduce the cross-talk to zero for the rate equation modeling. If the lower singlet to diamond conduction band energy gap is about 570 nm (2.1 eV), the plot tells us that the shift needs to be about 0.3 eV lower to 1.8 eV, where the absorption cross section is zero. This is assumed to be within the capabilities of a standard electrode.

Figure 3 shows the results of two separate rate equation optimization calculations of optical spin contrast as a function of (a) green laser power and (b) green laser pulse duration for the pumping phase. For both calculations, all variables in the SCC protocol are optimized to give the largest contrast with the exception of these two variables which are incremented as shown on the x axis of each plot. The optimal green laser parameters maximize the shelving into the singlet state and the optimal ionization laser parameters maximize the ionization from the singlet state. The contrast is optimized at 33% when the ionization laser power and pulse time are maximized to fully ionize the defect and when the green pump laser has a medium power and pulse time to maximize shelving into the NV singlet states while minimizing quadratic ionization

during the pumping phase. This result is higher than conventional NV optical cycling (25% [23]) but not necessarily higher than other established room temperature SCC protocols [20].

III. COMPARISON TO ESTABLISHED METHODS

Another SCC protocol that operates at ambient conditions comes from Jaskula *et al.* [20]. In their work, they ionize $m_s = 0$ population out of the ground state triplet state using two-step 637 nm quadratic ionization. In this protocol, $m_s = \pm 1$ population is shielded from ionization via the intersystem crossing. While their results are experimental, we can put their protocol into a similar rate equation and optimize to find a contrast that is directly comparable to our method. See Supplemental Material A4 [25] for more details on this calculation [20,22,39]. The optimized optical contrast we calculated from the Jaskula method was 37%, which is a little higher than the experimentally achieved contrast reported at 36% and higher again than the predicted contrast produced in our method. This is likely due to the higher ionization cross section from the excited triplet compared to the singlet as the energy gap to the diamond conduction band is smaller.

Given that the method proposed by Jaskula *et al.* [20] does not require the added complexity of the electrode, it seems that their method is better in terms of both spin contrast and experimental simplicity. However, the technique proposed in this paper can be improved by using the same pulsing method proposed by Hopper *et al.* [21]. Contrast is improved by running the pump and ionization sequences more than once and optimizing the pulses for each run while leaving the initialization and charge state readout processes unchanged. The idea is that, during the pumping phase, some electron population in the $m_s = \pm 1$ state will decay radiatively to the ground state instead of taking the ISC pathway to the singlet states. This permits repetition of the pumping and ionization phase to increase the probability of pumping the population into the singlet for ionization. This is shown in Fig. 1(d) with the square brackets around the pumping and ionization phase; this sequence can be repeated N times before the readout phase. In each pumping phase, the laser can have different parameters to optimize to improve the process. Thus, if there is not an electron population in the singlet state in the first run, it might be in the second or third. The individual pump and ionization phases must be shorter than the lower singlet lifetime (≈200 ns [32]) to avoid electron population decaying via the lower intersystem crossing (^1E to $^3A_2$). However, the overall sequence can be longer than 200 ns as the ionization phases would stop any decay via this pathway. The upper limit on the overall time of the sequence would be the coherence time of the NV which can be microseconds or even milliseconds [40]. In practice, as more sequences are added, the likelihood of ionizing from the singlet increases which means that each subsequent run increases the contrast by smaller and smaller amounts as the probability of the electron population remaining in the triplet state gets smaller. See Supplemental Material A2 [25] for an example set of parameters of the pulse sequence [11,22,35–37]. The simulation showed a reasonable increase when adding up to three runs of the SCC protocol and that the increase in contrast for four or more runs is negligible.

For experimental simplicity, the pumping and ionization lasers are only optimized over different pulse durations for each run of the protocol and the laser powers are constant. Running this protocol with three pulses ($N = 3$) gives a spin optical contrast of 42%; this contrast is about 5% higher than the spin contrast calculated for the Jaskula *et al.* process [20]; however, it requires more experimental apparatus to achieve (the electrode). It is worth noting that repeat pulsing is not possible using the method considered in Jaskula *et al.* as the ionization and excitation both occur out of the triplet states.

To understand the optical contrast improvement, we can relate the change in spin optical contrast to sensitivity by using the dc magnetic sensitivity from Rhondin *et al.* as an example [41]:

$$\eta_{dc} \sim \frac{1}{g\mu_B} \frac{1}{C\sqrt{nT_2^*}}, \qquad (2)$$

where g is the g factor for the magnetic moment, μ_B is the Bohr magneton, and $n = t_l * P$ is the optical collection efficiency defined by the total counts obtained from the NV, P, and the time of the readout t_l. T_2^* is the NV electronic spin dephasing time and C is the optical contrast. In principle, all the factors are constant except for the change in contrast, so the improvement in sensitivity is proportional to $1/C$. By subtracting the difference in the inverse contrast of one method to the other, we can predict that the Jaskula method offers an improvement in dc magnetic sensitivity of ≈ 1.2, compared to conventional optical cycling. The method in this paper offers an improvement in sensitivity of ≈ 1.6.

IV. DISCUSSION

The electrode-based SCC method presented in this work, while showing a mild improvement over other protocols, represents the highest optical spin contrast reported in the NV at ambient conditions. While this method does modestly improve optical spin contrast, the real advantage lies in its potential capabilities. In the previous section, the electrode was only activated during the ionization phase of the protocol to change the energy gap from the singlet to the ionized state. To alter the quadratic ionization process from the triplet states, the SCC protocol would involve a two-step electrode potential as opposed to the single potential used in the previous section. An example of the two-step potential is illustrated in Fig. 4. In the two-step potential, the electrode would initially have a negative potential (blue) for the pumping phase [Fig. 4(a)], shifting the NV energy levels away from the conduction band and reducing the probability of triplet ionization. This is shown in Fig. 4(a) by the green laser arrow which cannot make the gap from the ^3E state to the ionized $^2E + e$ state. In the second step of the process [Fig. 4(b)], the ionization phase, the electron is in the singlet state and the electrode would have its polarity reversed. This creates a positive potential (red), shifting the NV levels towards the conduction band and improving the rate of photoionization from the singlet while reducing cross-talk.

The effect of the negative electrode potential would be to change the ratio of triplet absorption to ionization, σ. Figure 5 shows the optical spin contrast as a function of σ optimized over the laser parameters. The contrast is maximized when
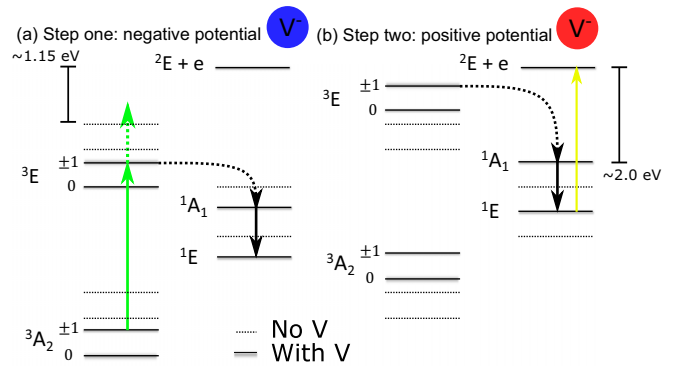

FIG. 4. Images of the NV under different electrode potentials. In (a), the electrode has a negative potential and shifts the energy levels away from the diamond conduction band (black lines compared to the dotted ones), reducing two-photon ionization due to the large energy gap from the excited triplet state. In (b) the electrode has a positive potential, shifting the NV energy levels closer to the diamond conduction band, increasing the rate of quadratic ionization as well as ionization from the singlet states.
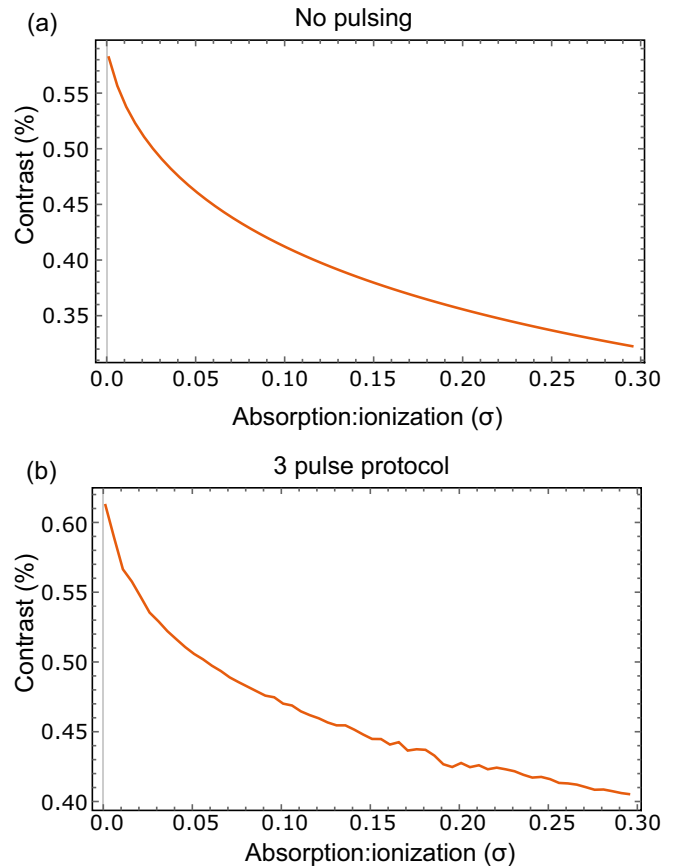

FIG. 5. Plots of the optical spin contrast as a function of changing absorption to photoionization ratio σ. The left image (a) is the optimization process with no pulsing of the laser protocol and the right image (b) is the same optimization but with the pulsing sequence repeated and optimized three times. In both cases, the contrast is maximized when $\sigma = 0$, i.e., no quadratic ionization, with a steady decline in contrast with increasing σ.

σ is zero, i.e., when there is no ionization process out of the triplet states. When $\sigma = 0$, the green laser pumping is maximized along with the ionization laser and its pulse duration is short. In Fig. 5(a), there is no pulsing system and the contrast maximizes at 58%; in Fig. 5(b) there is a three-pulse system and the contrast raises to 61%. Without triplet ionization, the main limitation of the optical spin contrast is the branching ratio at the ISC.

By using Eq. (2), an optical spin contrast of 61% translates to a 2.36-fold improvement in the NV sensitivity compared to conventional ODMR optical cycling techniques. However, using the electrode to alter the rate of quadratic ionization has other added benefits. In a publication by Doi *et al.* [42], they postulate that improving the ratio of NV^- to NV^0 during optical illumination would improve the number of photons the NV emits during a quantum operation. This was achieved in Doi *et al.* using dopants, but can be accomplished on single or ensemble NVs using an electrode by reducing the amount of triplet ionization. Another consideration when using the electrode for charge state control is the effect it might have on the spin coherence time of the NV. In most modern theories of the NV, spin decoherence occurs as the spin state in the NV interacts with nearby paramagnetic defects in the diamond which cause a spin flip in an NV electronic state [11,40]. Thus most efforts to improve NV coherence time involve engineering diamond samples that remove these paramagnetic defects. However, if the NV ionizes due to an unwanted ionization from the spin triplet, then the spin information of the NV is lost along with its charge state, effectively creating decoherence. This can be compounded by the fact that an increase in ionization and recombination attracts a local density of holes near the NV^- which can interact and cause further ionizations due to hole capture, even when there is no laser turned on for photoionization. Electrode-based charge state control can help reduce the number of photoionizations while providing a potential that repels local holes around the NV. While this concept could increase the spin coherence time for near-surface NVs, the effect of an electrode at this distance (10 nm) has been known to decrease spin coherence time [43], so extra work will need to be performed to understand the overall effect of the electrode potential on the NV spin coherence time.

The major issue with using the electrode to eliminate triplet ionization is the unpredictable nature in which the NV energy levels react to such a large electrode potential. The idea is to shift the gap such that the minimum energy gap for quadratic ionization is larger than the energy being used to excite the NV

during the pumping phase. With a green 532 nm laser (about 2.3 eV) and a minimum energy onset for photoionization from the excited triplet ^3E state (1.15 eV; see Fig. 4) [22], the electrode would have to shift the NV energy levels about 1.15 eV further away from the conduction band or half the energy of the excitation laser itself. It is unclear what such a large potential would do to the NV energy levels or whether they would shift linearly with electric potential at such large values. This could be solved using density functional theory (DFT) calculations [44].

V. CONCLUSION

The modeling performed in this paper shows a relatively straightforward way to improve NV optical spin contrast in ambient conditions through careful manipulation of optical pulses in an SCC protocol. With the pulsing mechanism in place, the 42% contrast calculated promises a 1.6-fold increase in the NV dc magnetic field sensitivity, which is a significant improvement on other mechanisms and has applications in quantum sensing, quantum computation, and experiments to understand NV energy levels in a variety of conditions. The electrode itself has many other potential advantages such as improving optical photoluminescence and coherence time. As a result, there is a lot of future work to be done with the electrode. This includes the experimental realization of the initial one-step potential SCC protocol and experimental investigations of the possible two-step potential SCC protocol. Further theoretical modeling of the effects of high potentials on the NV energy levels is required as well as further experimental and theoretical investigations of the effects of the electrode on the NV charge state stability and its effect on the NV fluorescence and coherence. The results shown so far demonstrate concrete theoretical evidence of NV performance enhancement that is applicable in a variety of quantum technologies and future work has great promise for a variety of alternative means of NV performance enhancement.

[1] J. F. Barry, M. J. Turner, J. M. Schloss, D. R. Glenn, Y. Song, M. D. Lukin, H. Park, and R. L. Walsworth, Optical magnetic detection of single-neuron action potentials using quantum defects in diamond, Proc. Natl. Acad. Sci. USA **113**, 14133 (2016).

[2] G. Kucsko, P. C. Maurer, N. Y. Yao, M. Kubo, H. J. Noh, P. K. Lo, H. Park, and M. D. Lukin, Nanometre-scale thermometry in a living cell, Nature (London) **500**, 54 (2013).

[3] D. Le Sage, K. Arai, D. R. Glenn, S. J. Devience, L. M. Pham, L. Rahn-Lee, M. D. Lukin, A. Yacoby, A. Komeili,

and R. L. Walsworth, Optical magnetic imaging of living cells, Nature (London) **496**, 486 (2013).

[4] M. S. Barson, L. M. Oberg, L. P. McGuinness, A. Denisenko, N. B. Manson, J. Wrachtrup, and M. W. Doherty, Nanoscale vector electric field imaging using a single electron spin, Nano Lett. **21**, 2962 (2021).

[5] M. Lesik, T. Plisson, L. Toraille, J. Renaud, F. Occelli, M. Schmidt, O. Salord, A. Delobbe, T. Debuisschert, L. Rondin, P. Loubeyre, and J.-F. Roch, Magnetic measurements on micrometer-sized samples under high pressure using designed NV centers, Science **366**, 1359 (2019).

[6] P. C. Maurer, G. Kucsko, C. Latta, L. Jiang, N. Y. Yao, S. D. Bennett, F. Pastawski, D. Hunger, N. Chisholm, M. Markham, D. J. Twitchen, J. Ignacio Cirac, and M. D. Lukin, Room-temperature quantum bit memory exceeding one second, Opt. InfoBase Conf. Papers **336**, 1283 (2012).

[7] Y. Wu, Y. Wang, X. Qin, X. Rong, and J. Du, A programmable two-qubit solid-state quantum processor under ambient conditions, npj Quantum Inf. **5**, 9 (2019).

[8] A. P. Nizovtsev, S. Y. Kilin., F. Jelezko, T. Gaebal, I. Popa, A. Gruber, and J. Wrachtrup, A quantum computer based on NV centers in diamond: Optically detected nutations of single electron and nuclear spins, Opt. Spectrosc. (English translation of Opt. Spektrosk.) **99**, 233 (2005).

[9] L. Childress and R. Hanson, Diamond NV centers for quantum computing and quantum networks, MRS Bull. **38**, 134 (2013).

[10] S. Pezzagna and J. Meijer, Quantum computer based on color centers in diamond, Appl. Phys. Rev. **8**, 011308 (2021).

[11] M. W. Doherty, N. B. Manson, P. Delaney, F. Jelezko, J. Wrachtrup, and L. C. Hollenberg, The nitrogen-vacancy colour centre in diamond, Phys. Rep. **528**, 1 (2013).

[12] T. M. Babinec, B. J. Hausmann, M. Khan, Y. Zhang, J. R. Maze, P. R. Hemmer, and M. Lončar, A diamond nanowire single-photon source, Nat. Nanotechnol. **5**, 195 (2010).

[13] P. Siyushev, F. Kaiser, V. Jacques, I. Gerhardt, S. Bischof, H. Fedder, J. Dodson, M. Markham, D. Twitchen, F. Jelezko, and J. Wrachtrup, Monolithic diamond optics for single photon detection, Appl. Phys. Lett. **97**, 241902 (2010).

[14] P. Appel, E. Neu, M. Ganzhorn, A. Barfuss, M. Batzer, M. Gratz, A. Tschöpe, and P. Maletinsky, Fabrication of all diamond scanning probes for nanoscale magnetometry, Rev. Sci. Instrum. **87**, 063703 (2016).

[15] N. H. Wan, B. J. Shields, D. Kim, S. Mouradian, B. Lienhard, M. Walsh, H. Bakhru, T. Schröder, and D. Englund, Efficient extraction of light from a nitrogen-vacancy center in a diamond parabolic reflector, Nano Lett. **18**, 2787 (2018).

[16] N. Aslam, G. Waldherr, P. Neumann, F. Jelezko, and J. Wrachtrup, Photo-induced ionization dynamics of the nitrogen vacancy defect in diamond investigated by single-shot charge state detection, New J. Phys. **15**, 013064 (2013).

[17] L. Hanlon, L. Oberg, Y. Chen, and M. W. Doherty, Spin-to-Charge Conversion with Electrode Confinement in Diamond, Phys. Rev. Appl. **16**, 064050 (2021).

[18] D. M. Irber, F. Poggiali, F. Kong, M. Kieschnick, T. Lühmann, D. Kwiatkowski, J. Meijer, J. Du, F. Shi, and F. Reinhard, Robust all-optical single-shot readout of nitrogen-vacancy centers in diamond, Nat. Commun. **12**, 532 (2021).

[19] Q. Zhang, Y. Guo, W. Ji, M. Wang, J. Yin, F. Kong, Y. Lin, C. Yin, F. Shi, Y. Wang, and J. Du, High-fidelity single-shot readout of single electron spin in diamond with spin-to-charge conversion, Nat. Commun. **12**, 1529 (2021).

[20] J. C. Jaskula, B. J. Shields, E. Bauch, M. D. Lukin, A. S. Trifonov, and R. L. Walsworth, Improved Quantum Sensing with a Single Solid-State Spin via Spin-to-Charge Conversion, Phys. Rev. Appl. **11**, 064003 (2019).

[21] D. A. Hopper, R. R. Grote, A. L. Exarhos, and L. C. Bassett, Near-infrared-assisted charge control and spin readout of the nitrogen-vacancy center in diamond, Phys. Rev. B **94**, 241201(R) (2016).

[22] L. Razinkovas, M. Maciaszek, F. Reinhard, M. W. Doherty, and A. Alkauskas, Photoionization of negatively charged NV centers in diamond: Theory and *ab initio* calculations, Phys. Rev. B **104**, 235301 (2021).

[23] G. Balasubramanian, P. Neumann, D. Twitchen, M. Markham, R. Kolesov, N. Mizuochi, J. Isoya, J. Achard, J. Beck, J. Tissler, V. Jacques, P. R. Hemmer, F. Jelezko, and J. Wrachtrup, Ultra-long spin coherence time in isotopically engineered diamond, Nat. Mater. **8**, 383 (2009).

[24] M. Fox, *Quantum Optics: An Introduction*, 6th ed. (Oxford University Press, Oxford, 2009).

[25] See Supplemental Material at http://link.aps.org/supplemental/ 10.1103/PhysRevB.107.134111 for further details on calculations.

[26] G. Waldherr, J. Beck, M. Steiner, P. Neumann, A. Gali, T. Frauenheim, F. Jelezko, and J. Wrachtrup, Dark States of Single Nitrogen-Vacancy Centers in Diamond Unraveled by Single Shot NMR, Phys. Rev. Lett. **106**, 157601 (2011).

[27] R. Ulbricht and Z. H. Loh, Excited-state lifetime of the NV infrared transition in diamond, Phys. Rev. B **98**, 094309 (2018).

[28] D. A. Hopper, J. D. Lauigan, T. Y. Huang, and L. C. Bassett, Real-Time Charge Initialization of Diamond Nitrogen-Vacancy Centers for Enhanced Spin Readout, Phys. Rev. Appl. **13**, 024016 (2020).

[29] J. P. Tetienne, L. Rondin, P. Spinicelli, M. Chipaux, T. Debuisschert, J. F. Roch, and V. Jacques, Magnetic-field-dependent photodynamics of single NV defects in diamond: An application to qualitative all-optical magnetic imaging, New J. Phys. **14**, 103033 (2012).

[30] N. Kalb, P. C. Humphreys, J. J. Slim, and R. Hanson, Dephasing mechanisms of diamond-based nuclear-spin memories for quantum networks, Phys. Rev. A **97**, 062330 (2018).

[31] U. Keller, *Ultrafast Lasers. A Comprehensive Introduction to Fundamental Principles with Practical Applications*, 1st ed. (Springer Nature Switzerland AG, Cham, 2021).

[32] V. M. Acosta, A. Jarmola, E. Bauch, and D. Budker, Optical properties of the nitrogen-vacancy singlet levels in diamond, Phys. Rev. B **82**, 201202(R) (2010).

[33] A. Safarpour, F. Dehnavi, M. Saberi, R. Lotfi, and W. A. Serdijn, Speed-power improvement in high-voltage switches employed in multielectrode arrays, IEEE Trans. Circuits Syst. II: Express Briefs **69**, 3139 (2022).

[34] S. Menzel, M. Von Witzleben, V. Havel, and U. Böttger, The ultimate switching speed limit of redox-based resistive switching devices, Faraday Discuss. **213**, 197 (2019).

[35] G. Davies, Vibronic spectra in diamond, J. Phys. C **7**, 3797 (1974).

[36] K. Huang and A. Rhys, Theory of light absorption and non-radiative transitions in F-centres, R. Soc. **204**, 74 (1950).

[37] P. Kehayias, M. W. Doherty, D. English, R. Fischer, A. Jarmola, K. Jensen, N. Leefer, P. Hemmer, N. B. Manson, and D. Budker, Infrared absorption band and vibronic structure of the nitrogen-vacancy center in diamond, Phys. Rev. B **88**, 165202 (2013).

[38] L. Razinkovas, M. W. Doherty, N. B. Manson, C. G. Van de Walle, and A. Alkauskas, Vibrational and vibronic structure of isolated point defects: The nitrogen-vacancy center in diamond, Phys. Rev. B **104**, 045303 (2021).

[39] K. M. C. Fu, C. Santori, P. E. Barclay, L. J. Rogers, N. B. Manson, and R. G. Beausoleil, Observation of the Dynamic

Jahn-Teller Effect in the Excited States of Nitrogen-Vacancy Centers in Diamond, Phys. Rev. Lett. **103**, 256404 (2009).

[40] E. D. Herbschleb, H. Kato, Y. Maruyama, T. Danjo, T. Makino, S. Yamasaki, I. Ohki, K. Hayashi, H. Morishita, M. Fujiwara, and N. Mizuochi, Ultra-long coherence times amongst room-temperature solid-state spins, Nat. Commun. **10**, 3766 (2019).

[41] L. Rondin, J.-P. Tetienne, T. Hignant, J.-F. Roch, P. Maletinsky, and V. Jacques, Magnetometry with nitrogen-vacancy centers in diamond, Rep. Prog. Phys. **77**, 056503 (2014).

[42] Y. Doi, T. Fukui, H. Kato, T. Makino, S. Yamasaki, T. Tashima, H. Morishita, S. Miwa, F. Jelezko, Y. Suzuki, and N. Mizuochi, Pure negatively charged state of the NV center in n-type diamond, Phys. Rev. B **93**, 081203(R) (2016).

[43] A. Ariyaratne, D. Bluvstein, B. A. Myers, and A. C. Jayich, Nanoscale electrical conductivity imaging using a nitrogen-vacancy center in diamond, Nat. Commun. **9**, 2406 (2018).

[44] R. W. Nunes and X. Gonze, Berry-phase treatment of the homogeneous electric field perturbation in insulators, Phys. Rev. B **63**, 155107 (2001).